Available online at www.sciencedirect.com

ScienceDirect

Procedia CIRP 110 (2022) 289–294

www.elsevier.com/locate/procedia

V CIRP Conference on Biomanufacturing

Design and Manufacturing of Bone-like Composites

Cuneo, A.[a,b‡], Timossi, F.[a,b‡], Musenich, L.[a], Stagni, A.[a], Wilhelm, F.[b*], Libonati, F.[a†]

[a]*University of Genoa, via all'Opera Pia 15A, 16145, Genoa, Italy*
[b]*Fraunhofer Institute for Casting, Composite and Processing Technology IGCV, Am Technologiezentrum 2 | 86159 Augsburg, Germany*
[‡]*equally-contributing authors*

Abstract

Bone is a complex structural composite that features a remarkable combination of mechanical properties, in spite of its rather meager building blocks (i.e., mineral and proteins). The reasons behind these optimal mechanical performances lay in bone hierarchical organization. A crucial role is played by the microscale structure (Haversian), which is formed by a repetition of cylindrical building blocks (osteons) surrounded by a matrix of interstitial tissue. Following a biomimetic approach, mimicking this natural architecture in the design of innovative fiber-reinforced composites appears to be a very promising way to improve the performance of engineering composites. However, it is still an open challenge due to manufacturing-induced limitations. Here we aim to overcome such limitations and implement a bone-like design into novel fiber-reinforced materials. We first focus on the design and manufacturing of osteon-like features by pull-winding technology, to get a continuous and rapid production. We fabricate osteon-inspired multilayer concentric rods by coupling multiple layers of fibers, characterized by different materials and orientations. To study the effect of each layer on the overall mechanical properties and provide guidelines for optimal design, we perform finite element simulations. The simplicity and versality of the production line allow us to manufacture great quantities of these rods at a high production rate. The combination of finite elements analysis and experimental design allow us to find a trade-off between the best and the most feasible configuration. Future works will focus on the manufacturing of a multiscale composite laminate made of these small pull-winded rods, inspired by the osteons.

Keywords: biomimetics; bone; osteon; pull-winding

Introduction

Fiber reinforced composites (FRC) are becoming more and more used nowadays thanks to their high strength and stiffness that, combined with a low density, allow one to obtain lightweight parts with excellent mechanical performances [1]. Yet, a strong limitation of these material is their poor damage tolerance, an essential property especially in structural application, where safety is considered one of the major priorities. Therefore, in the last few years, a lot of studies have been focused on the design and manufacturing of bio-inspired FRCs, whose structures mimic those of natural structural materials. Natural tissues, indeed, are composites with a hierarchical structure that has been developed and improved over billions of years. This allows them to have mechanical properties, such as strength

[†] Corresponding author. Tel.: +39-010-3352846; *E-mail address:* flavia.libonati@unige.it
[*] Co-corresponding author. Tel.: +49-821-90678-246; *E-mail address:* frederik.wilhelm@igcv.fraunhofer.de

10.1016/j.procir.2022.06.052

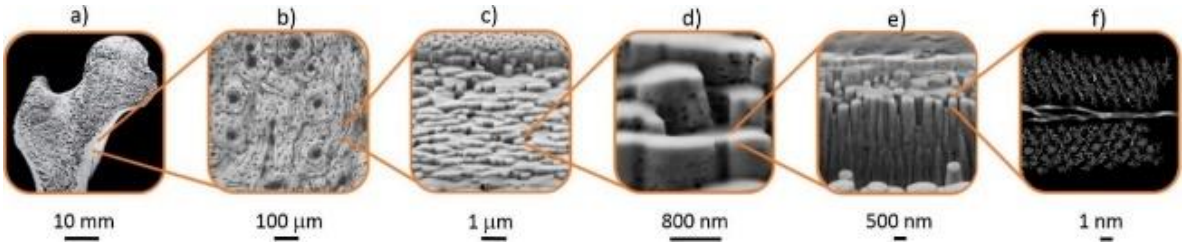

Fig. 1 - Bone hierarchical structure at different length scales. (a) Bone macrostructural level: here it can be distinguished in cortical (or compact) tissue and trabecular tissue (aka spongy or cancellous) (b) Microstructural level of cortical bone, also known as Haversian structure, characterized by the presence of the typical cylindrical feature (i.e., osteon) (c) Circumferential lamellae. (d) Collagen fiber bundles. (e) Mineralized collagen fibrils. (f) Single tropocollagen molecule surrounded by hydroxyapatite nanocrystals. The image represented in (b) was taken using an optical microscope; the pictures shown in (c)–(e) were taken by means of an SEM after an FIB (focus ion beam) cutting; figure (f) is from atomistic simulations of collagen-hydroxyapatite system. Taken with permission from [21]

and toughness, both greater than those of their individual constituents and combined to achieve damage-tolerance and multiple functionalities. Bone is a typical example in this sense, featuring an optimal combination of remarkable mechanical properties. Bone is a biological composite with a hierarchical structure mainly composed of collagen, water, and hydroxyapatite crystals. Arrangements of these components into different functional units contribute to create a light and tough structure that is multi-functional and able to adapt to diverse mechanical environments [2]. Indeed, bone can activate two different kinds of toughening mechanisms at different length scales: intrinsic and extrinsic. The former, occurring at the sub-micro scale, promote ductility and protect the integrity of the entire structure through energy dissipation. The latter act instead as a shield to growing cracks [3]. Furthermore, as a living tissue, it has a unique capacity of self-repair, through growth and remodeling processes, which confers it a dynamic structure. Going from the nanoscale to the macroscale, different hierarchical levels can be found in bones (*Fig. 1*). A special focus deserves one of the most important structural elements of bone: the osteons. These are hollow cylinders with an external diameter of about 200-300 µm. They are made of concentric lamellae, with a thickness of 3-7 µm and whose number can go up to 20. Each lamella is composed of collagen fibrils that can assume different orientations: the specific pattern is optimized to have a better response against external loads [4]. The internal channel, called Haversian, has a diameter of 50-90 µm. The interconnection between each osteon is possible thanks to the presence of interstitial lamellae. Several works have been carried out in recent years with the aim of studying and reproducing bone structure and, in particular, bone microstructural organization. Among these, Libonati et *al.* [5]–[7] focused on the manufacturing of a laminate and a component that mimics the Haversian structure, while Vellwock at *al.* [8] focused on the numerical simulation of bone-like composites. The combination of simulation and experiments allowed for a design of novel FRCs with enhanced fracture toughness and an optimal combination of strength and stiffness. More recently, the design and manufacturing focused on the osteon features, leading to the design of osteon-like features (OLSs) through lamination and 3D-printing [9], [10]. In particular, the combination of numerical simulations, collagen microarchitecture mapping through Raman Spectroscopy, and 3D-printing was essential to evaluate the relationship between fibers orientation and mechanical properties of OLSs and to expose the role of different bone lamellar patterns occurring in different anatomical locations, i.e., tension- and compression-dominated regions [10]. Building on this work [10], the present research focuses on the manufacturing of OLSs optimized for tension- and compression-dominated loading conditions. The manufacturing technique is similar to the one adopted in [9], but aims to overcome size limitations. Indeed, the proposed technique allowed us to produce smaller OLSs with a higher production rate. Considering the promising results of a previous study by Grezzana et *al.* [10], we decided to manufacture two different OLS configurations: one that behaves better under compression and one that behaves better under tension, from now on called osteon A and osteon B, respectively. The implementation of these two kinds of OLSs into a laminate would allow one to obtain a material capable of bearing different kinds of loads, as it occurs in bones tissue. The whole composite will mimic the Haversian structure at a macroscale level, leading to a multiscale FRC. As a future perspective, the optimization of manufacturing and design parameters would yield novel multiscale composites tailored to meet specific loading conditions. In the following sections a description of the manufacturing process and the numerical analysis will be given. It has to be stressed that the final design of the OLSs has been constrained by manufacturing limitations. That is why, an overall knowledge of the process was necessary before performing finite element analyses.

1. Methods and materials

1.1. Pull-Winding Process

The manufacturing technique used in this project is a modification of traditional pultrusion and is called pull-winding. This technique is a combination of pultrusion and filament winding. Pultrusion itself is a continuous process for manufacturing of high performance FRC with constant cross-section [8],[9]. This process is characterised by a low labour content and high raw materials conversion efficiency at an attractive cost [13]. Intrinsically, pultrusion has a high unidirectional reinforcement in the haul-off direction, since rovings are mostly used as fiber material. For additional transverse reinforcement, textiles, such as mats, non-crimp fabrics or woven fabrics, can be used. However, this is only economically possible for parts having a profile dimension greater than 5 mm. Such limitation does not exist for pull-winding. The fibers are pulled from a roving unit through a resin bath and a die like in the pultrusion process. The pultruded profile is then wrapped by additional winding layers of fibers [14], [15]. From a manufacturing point of view, the foundations of this project are based on a previous

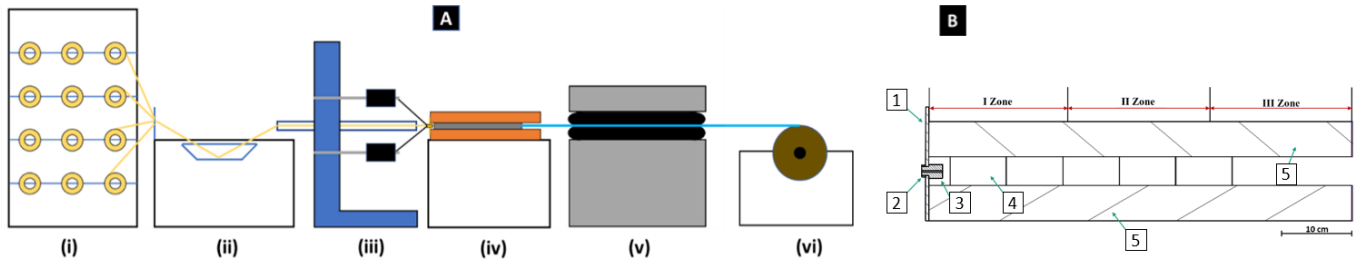

Fig. 2 - Set-up and details of the pultrusion line used for the manufacture of the OLSs. A) Schematization of the overall line: (i) Fiber rack of the unidirectional layer (ii) Resin bath: tank where fibers get impregnated (iii) Winding machine: rotating component that allows the fiber wrapping at the desired angle (iv) Heating system (v) Caterpillar: pulling component (vi) Spool. B) Heating system of the pultrusion line. The three heating zones are highlighted (1) Steel plate used as support for the nozzle, (2) Nut, (3) Brass nozzle used as mold, (4) Aluminium block, (5) Heating plate.

work conducted at Fraunhofer IGCV [16], whose outcome was the manufacturing of two layers OLSs. Since the goal of our work was the production of OLSs made of three layers and with different dimensions, some modifications have been introduced to that production line. *Fig. 2A* shows a schematic of the pultrusion line that we used. The main set-up changes mainly regarded the heating system. The latter is the most important component of a pultrusion line and it typically consists of a mold through which the reinforcing impregnated fibers pass. In this die, the curing of the resin system takes place under the action of heat, producing the desired profile geometry (*Fig. 2B*). The profile goes through a short nozzle, which fulfils the function of mold and gets the desired shape. After the profile passes between two rows of aluminium blocks, used for a better transfer of heat from the heating plates, and here it cures. As visible from *Fig. 2B* heating system is divided into three different heating zones, where each can be set to a different temperature. The latter depends on several parameters (translational velocity, type of fibers, cross-section dimensions) whose optimal combination was defined through a trial and error approach. Another process parameter, affected by several factors, is the travel speed of the profile (*Eq.1*):

$$v = \frac{n * D_1 * \pi}{\tan(\gamma)} \quad (1)$$

where *v, n, D_1* and γ are the caterpillar speed, the winding machine rotational speed, the inner layer diameter, and the desired winding angle, respectively. Once the diameter and the angle were fixed the correlation between the two velocities, *v* and *n*, could be found. Since the maximum rotational speed of the winding machine was 170 *round/min,* the production rate (dependent on the caterpillar speed) was limited.

1.2. OLS Manufacturing

Despite the initial idea of accurately mimicking the osteonic structure, several simplifications have been introduced in the final design due to manufacturing limitations. We fabricated OLSs with 3 concentric layers: the inner one is unidirectional (UD), while the outer ones have different winding angles according to the desired mechanical properties (see section *2.4*). The OLSs are manufactured without the inner hole: this is not a limitation of the pull-winding technique, but it was a decision necessary to produce 3 layers-OLS of such small dimensions. The first two layers are produced simultaneously. The UD fibers placed on the rack are pulled by the caterpillar through the resin bath where they get impregnated. They are, in this way, responsible for carrying the resin from the resin bath to the mold. Tensioning rods assure in the meantime an accurate fiber tension. Near the heating system, the UD-impregnated fibers serve as a mandrel around which the fibers of the winding machine are wound. All fibers pass through a nozzle and cure inside the heating system. Since we needed a continuous product, the OLS is wrapped around a spool (see *Fig. 2A*). To produce an OLS with three layers, the finished OLS with two layers was passed through the impregnation bath again in the same way as the UD fibers before and wrapped with a third layer. Referring to *Fig. 2A*, the osteon spool of the first process (vi) is in the second process positioned before the resin bath, replacing the fibers rack (i). If two winding machines are available, this process can be done in one step.

1.3. Materials Selection

Different materials have been used for both the UD and the winding layers. For the UD layer we opted for two different types of carbon fibers (CF): the CF-3K (Tex=200 g/km, density=1.76 g/cm3) and CF-6K (Tex=400 g/km, density=1.76 g/cm3), using them according to the dimensions diameter we wanted to have (3K and 6K indicated the number of filaments per tow). For example, to obtain a UD-layer diameter of 1 mm, one CF-3K and two CF-6K have been used, while to obtain a UD-layer diameter of 0.8 mm, one CF-3K and one CF-6K have been used. The OLSs with lower stiffness were manufactured by using GF (Tex=1200 g/km, density =2.62 g/cm3) as the UD-layer. This made the process easier and smoother and required less maintenance. As for the winding layer, the type of CF was chosen according to the winding angle desired: for small angles (about 15°) CF-6K have been used, while for angles between 15°- 45° CF-3K have been used. The optimal winding angle depends, in fact, on two factors: the diameter of the inner layer and the width of the winding fiber. For small angles, larger fibers were required not to have too many gaps, while for high angles narrower ones were required not to have too many overlaps. The effect of a not ideal winding angle is an irregular surface caused by the presence of gaps or overlaps. Overlaps also lead to an excessive friction force that can cause problems in the process. However, since our goal was to obtain precise angles, different from the ideal ones, the final product presented gaps or overlaps depending on the type of fibers used and the dimension of the inner diameter. The resin used is an epoxy resin characterized by low viscosity and long pot-life (Araldite

LY5385 epoxy and Aradur 917-1 hardener by Huntsman, with the addition of releasing agent and accelerators).

1.4. OLS design

Two different types of OLSs have been produced: compressive- and tensile-resistant, called osteon A and B, respectively. In order to determine the best design for both types and to evaluate how the mechanical response changes in the different configurations, numerical simulations have been performed using the software Abaqus/CAE. The studied configurations are shown in *Table 1*. In every configuration the fibers in the inner layer are longitudinally aligned. This choice is due to a manufacturing limitation known from the beginning.

Table 1 – Configurations implemented in numerical simulations. 0° refers to the axial direction.

	I configuration	II configuration	III configuration
Osteon A	0°/45°/-45°	0°/30°/45°	0°/30°/60°
Osteon B	0°/15°/30°	0°/15°/-15°	0°/0°/0°

Axial compressive and buckling simulations have been carried out in linear elastic regime on the three configurations of osteon A, while tensile simulations have been made on osteons B. All the configurations analysed present a GF/Epoxy UD layer and CF/Epoxy winding layers. The properties of these materials have been evaluated using [17] and listed in in *Table 2*. A fiber volume fraction of 60% has been considered for both materials.

Table 2 – Materials properties. E [MPa] = Young's Modulus; ν [-] = Poisson's ratio; G [MPa] = Shear Modulus. The subscript 1 indicates the direction parallel to the fiber orientation, while 2, 3 are the directions orthogonal to 1.

	E_1	E_2, E_3	ν_{12}, ν_{13}	ν_{23}	G_{12}, G_{13}, G_{23}
CF/Epoxy	167200	9787	0.26	0.015	3421
GF/Epoxy	46000	9250	0.26	0.052	3453

The model used for compressive and tensile simulations is represented by a quarter of cylinder: indeed, the use of the symmetry allowed us to have a smaller number of elements in the numerical simulations. The cross-section dimensions replicate the experimental ones, while the length was arbitrary chosen following an assumption of elastic response. The type of elements used in these analyses is a C3D20R (general purpose quadratic brick element, with reduced integration). The type of mesh is structured: since the geometry of the model is quite simple, it can be discretized with elements of regular shape and size that are easy to control. The number of elements through each layer thickness was set to be at least equal to three. This choice, followed by a mesh sensitivity analysis, led to a final mesh composed by: 176325 nodes for the compressive model, 207984 nodes for the tensile model and 66211 nodes for the buckling model. The geometrical dimensions of the models are:

- Osteon A: $r_1=0.465$; $r_2=0.65$; $r_3=0.85$; $L=200$
- Osteon B: $r_1=0.465$; $r_2=0.70$; $r_3=0.90$; $L=200$

where r_1, r_2 and r_3 (in millimetres) are the radius associated to the first, second, and third layer, respectively.

Loads and boundary conditions in the compressive and tensile simulations have been chosen to replicate the real experimental set-up: one surface is clamped, while on the other a force of 500 N is applied in tension and compression, respectively. The buckling model is instead a full cylinder: this choice allowed us to also evaluate the deformation modes outside the plane of symmetry. The cross-section is the same one used for the compressive model, while the length is chosen to have the same slenderness ratio (SR) of osteons in the original bone, calculated with the following equation

$$SR = \frac{L}{K} = \frac{2}{\sqrt{\frac{I}{A}}} = \frac{2}{\sqrt{\frac{{D_e}^2 + {D_i}^2}{16}}} \sim 37 \qquad (2)$$

where L is the osteon length, which is approximately 2 mm [18], K is the radius of gyration and D_e and D_i are the external and internal osteon diameter whose values are 0.2 mm and 0.08 mm, respectively. After imposing the same slenderness ratio to our model, whose external diameter is 1.7 mm, we obtained a length of 16 mm. Loads and boundary conditions applied to the model are chosen to replicate those of one of the Euler's critical load cases: the pin-encastre. The type of analysis performed is a Linearized Pre-Buckling (LPB) simulation, which calculates the critical buckling loads on the basic hypothesis of linear response of the model. The results are then based upon macroscopic elastic effects and do not take into consideration microscopic problems, such as fiber buckling.

2. Results and Discussion

2.1. Manufacturing results

The manufactured OLSs are shown in the *Table 3*. The use of the pull-winding process allowed us to realize an FRC with a higher control on the fiber orientation and on the final layup, also maintaining our dimensional constraints (i.e., small osteon diameter). As a consequence, the mechanical properties in other directions than the pulling one (for example, circumferential and radial directions) are improved. As it can be seen, the tensile and compressive resistant OLS configurations realized are the [0°/15°/30°] and the [0°/30°/45°]. Regarding Osteon A, in fact, the [0°/30°/60°] configuration would have required excessively long times for the realization of the 60° layer. This is clearly visible from *Eq.1*: the higher γ, the lower *v,* considering that *n* is limited. For what concerns the configurations with a negative angle (i.e., [0°/45°/-45°] and [0°/15°/-15°]) these were not doable at the time due to the impossibility of inverting the rotational speed of the winding machine. All these manufacturing limitations led in the end to the realization of the previously mentioned configurations which can be seen as a compromise between what we desired to produce and what we were able to produce.

After the final set-up was designed, the production has been focused on Osteon A_1, B_1 and A_2. The presence of the UD layer made of CF makes Osteon A_1 and B_1 the best OLSs realized in

Table 3 – Lists of the manufactured OLS configurations. Amount of fibers mentioned within the brackets.

	I Layer	II Layer	III Layer
Osteon A_1	0° CF-3K (1) + CF-6K (2)	30° CF-3K (1)	45° CF-3K (1)
Osteon B_1	0°CF-3K (1) + CF-6K (1)	15° CF-6K (1)	30° CF-3K (1)
Osteon A_2	0° GF (1)	30° CF-3K (1)	45° CF-3K (1)
Osteon B_2	0° GF (1)	15° CF-6K (1)	30° CF-3K (1)

terms of mechanical properties, while Osteon A_2 represents the best configuration in terms of flexibility. In view of embedding these osteons into a bone-inspired multiscale composite laminate, each OLS needed to be more than 100 m long: the modifications made on the previous pultrusion line have been the key to produce such a big number of meters using a continuous process. In particular, the use of a short nozzle allowed us to reduce the friction area between the fibers and the nozzle itself, thus allowing a higher speed to be reached. A maximum velocity of 0.9 m/min was achieved. It has to be highlighted that, on the other hand, the open-air curing, consequence of the nozzle short length, led to the manufacturing of a product with a rough surface (i.e., the external diameter was variable along all the product) and greater cross-section dimensions than the theoretical ones. For this reason, the real fiber volume fractions of the individual layers are probably lower than the theoretical values for the UD and winding layers (65% and 60%, respectively). Thus, lower mechanical properties are also then expected.

2.2. Numerical results

The most important results considered for Osteon A are the compressive stiffness, calculated as stress/strain (MPa), and the critical buckling load, calculated as the eigenvalue that comes as the result of a buckling analysis with a unitary force. Results for the compressive simulations are shown in *Fig. 3*.

Fig. 3A shows that the best configuration appears to be the [0°/30°/60°]: it has, in fact, the highest compressive stiffness. In order to determine the best configuration for Osteon A an evaluation of the stress distribution in the thickness of the model has been also made. The results are visible in *Fig. 4*, where a cylindrical coordinate system has been used. An interesting result is that the radial stress in the [0°/30°/60°] configuration is negative: this can be seen as a natural constraint against the radial expansion that characterizes the buckling phenomenon and a hypothetical crack growth. This behavior could be compared to a natural toughening mechanism of bones (i.e., constrained microcracking). *Fig. 4* also shows that the [0°/45°/-45°] configuration has the most heterogeneous stress distribution. This behavior, that can be linked to the high angular difference between the second and third layer (90°), helps in terms of structural instability and reduces delamination issues [19].

Regarding Osteon B the most important result is instead the tensile stiffness: this is shown in *Fig. 3B*. As expected the stiffest configuration is the [0°/0°/0°], which was not manufactured due to pull-winding manufacturing constraints. Indeed, staying on the same angle for large thickness radius without periodically varying it may create some kind of instability and larger maximum stresses through the overall thickness [19].

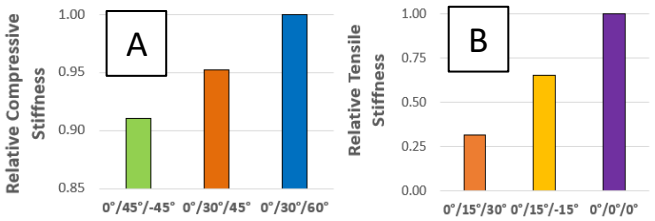

Fig. 3 – Uniaxial compressive (A) and tensile (B) results of OLSs. Simulation results are normalised with respect to the maximum value to allow a direct comparison in terms of compressive stiffness.

The best tensile configuration, which also matches the manufacturing constraints, is then the [0°/15°/30°] one. Finally, the critical loads from the buckling analysis are reported. They are then compared with the critical loads, P_{cr}, estimated using Euler's critical load formula for the pin-encaster case:

$$P_{cr} = \frac{\pi^2 * E * J}{(\alpha * l)^2} \tag{3}$$

where E is the Young's modulus, J is the minimum area moment of inertia, α is the column effective length factor ($\alpha = 0.7$ for our boundary conditions), and l is the model length. This estimation was only used in order to validate our models. In fact, Euler's formula is referred to a homogeneous and isotropic material with a constant cross-section geometry, while OLSs are anisotropic composites. These results are shown in *Fig. 5*, where ε_r is the relative error between the numerical and the analytical critical load values. The relative error is relatively high for every configuration. This is due to the several approximations of the Euler's formula, previously mentioned. However, the relative error is basically the same in each configuration, allowing the FE-models to replicate the analytical trend. Another important outcome of this graph is that the critical load of the [0°/30°/60°] configuration is the highest. Considering both the results from the compressive and the buckling simulations, this configuration is then the one with the best response under a compression load. As it was expected, the more the fibers are aligned along the cylinder axis, the higher the tensile stiffness. On the contrary, placing the fibers along the circumferential direction improves the compressive behaviour. In fact, these configurations limit the radial deformation and this delays the buckling failure [10]. Moreover, having fibers oriented perpendicular to the main loading direction can be used to enhance strength and energy absorption [20].

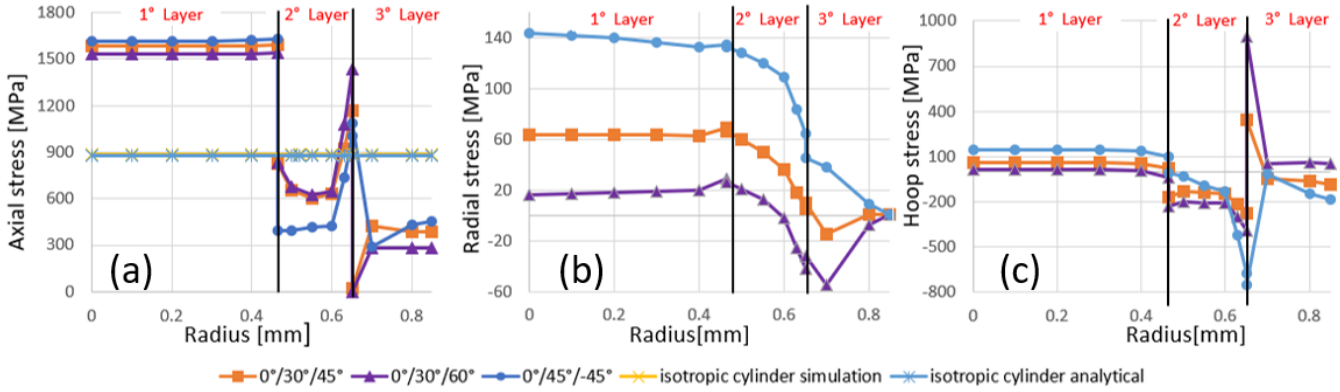

Fig. 4 – Stress distribution of Osteon A evaluated along a node path located in the mid-length of the model, in radial direction. **(a)** Axial stress in absolute value, **(b)** radial stress **(c)** hoop stress.

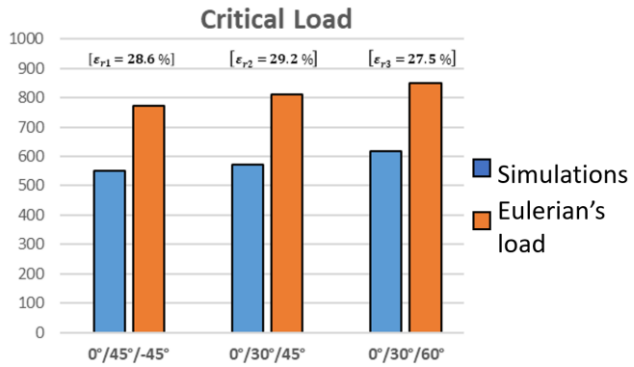

Fig. 5 – Comparison between the numerical and the analytical critical load

3. Conclusions

This work focuses on the manufacturing of materials whose structure is inspired by the cylindrical microstructural features characteristic of bone tissue and, in particular, of the Haversian system, the osteons. The use of the pull-winding process allows one to obtain products of limited size and composed by several stacked layers. Fibers in each layer are oriented along different angles that, in this work, range from 0° (i.e. longitudinal direction) to 45°. Higher angles can be reached with the use of smaller fibers. The final configurations realized represent a tradeoff between the results of numerical simulations and the manufacturing-induced limitations. Two different types of OLSs have been realized: one behaves better under tension and the other one under compression. A good result has been obtained in terms of production rate and of product-length manufactured continuously. This was possible also thanks to the modifications applied to the previous set-up of the pultrusion line. On the other hand, the same changes led to the manufacturing of a profile characterized by a rough external surface, which could be more difficult to be embedded into a multiscale composite laminate. In future works, the OLSs with GF in the UD-layer will be inserted into a textile that will be pultruded successively to fabricate a final laminate. Their great flexibility was, in fact, an essential requirement for their insertion into a textile. Instead, the osteons containing CF in the UD-layer will be used to fabricate a laminate by a manual lamination technique and cured through the VARTM process. Finally, a mechanical campaign will be carried out in order to evaluate the mechanical properties of the produced OLSs and the mechanical response of the multiscale laminates to different loading conditions.

Acknowledgements

F.L. acknowledges support from the University of Genoa under the Curiosity Driven Starting Grant 2020 initiative.

References

[1] Chawla KK, Composite Materials Science and Engineering. 2012.
[2] Haghighi P, Structure, function and adaptation of compact bone, Skeletal Radiol., vol. 18, no. 7, p. 506, 1989.
[3] Kapat K and Dhara S, Biopolymers Modification and Their Utilization in Biomimetic Composites for Osteochondral Tissue Engineering, in Handbook of Composites from Renewable Materials, 2017, pp. 253–285..
[4] Skedros JG, Keenan KE, Williams TJ, and Kiser CJ, Secondary osteon size and collagen/lamellar organization (‘ osteon morphotypes’) are not coupled, but potentially adapt independently for local strain mode or magnitude, J. Struct. Biol., vol. 181, no. 2, pp. 95–107, 2013.
[5] Libonati F, Vellwock AE, Ielmini F, Abliz D, Ziegmann G, and Vergani L, Bone-inspired enhanced fracture toughness of de novo fiber reinforced composites, Sci. Rep., vol. 9, no. 1, 2019.
[6] Libonati F, Colombo C, and Vergani L, Design and characterization of a biomimetic composite inspired to human bone, Fatigue Fract. Eng. Mater. Struct., vol. 37, no. 7, 2014.
[7] Libonati F et al., Squeeze-winding: A new manufacturing route for biomimetic fiber-reinforced structures, Compos. Part A Appl. Sci. Manuf., vol. 132, no. December 2019, 2020.
[8] Vellwock AE, Vergani L, and Libonati F, A multiscale XFEM approach to investigate the fracture behavior of bio-inspired composite materials, Compos. Part B Eng., vol. 141, pp. 258–264, 2018.
[9] Trevisan G, Numerical And Experimental Design Of An Osteon-Like Structure, 2019.
[10] Grezzana G, Loh HC, Qin Z, Buehler MJ, Masic A, and Libonati F, Probing the Role of Bone Lamellar Patterns through Collagen Microarchitecture Mapping, Numerical Modeling, and 3D-Printing, Adv. Eng. Mater., vol. 22, no. 10, Oct. 2020.
[11] Starr TF, Pultrusion for engineers. Abington, 2000.
[12] R. W. Meyer, Handbook of Pultrusion Technology. London, 1985.
[13] Shaw-Stewart D and Sumerak JE, The pultrusion process. Woodhead Publishing Limited, 2000.
[14] Brack A, Brecher C, Emonts M, and Eckert M, Micro-Pullwinding - An automated production technology for medical devices. 2013.
[15] Wasiak C, Nettleton D, Jannsen H, and Brecher C, Quantification of micro-pullwinding process as basis of data mining algorithms for predictive process model, 2017.
[16] Weidenhiller J, Entwicklungsstudie zur Herstellung einer bionischen Rohrstruktur mittels Pultrusion. 2021.
[17] MECH-Gcomp.
[18] Bonewald LF, Osteocyte Biology, Osteoporos. Fourth Ed., pp. 209–234, 2013.
[19] Elgohary MH, El-Geuchy MI, Abdallah HM, and Sayed SS, Stress analysis of multi-layered composite cylinders subjected to various loadings, IOP Conf. Ser. Mater. Sci. Eng., vol. 1172, no. 1, p. 012005, 2021.
[20] Zorzetto L and Ruffoni D, Wood-Inspired 3D-Printed Helical Composites with Tunable and Enhanced Mechanical Performance, Adv. Funct. Mater., vol. 29, no. 1, pp. 1–9, 2019.
[21] Libonati F and Vergani L, Understanding the structure–property relationship in cortical bone to design a biomimetic composite, Compos. Struct., vol. 139, pp. 188–198, Apr. 2016,